Effect of size on the surface energy of noble metal nanoparticles from analytical and numerical approaches

Hakim Amara, Jaysen Nelayah, Jérôme Creuze, Adrian Chmielewski, Damien Alloyeau, Christian Ricolleau, Bernard Legrand

Effect of size on the surface energy of noble metal nanoparticles from analytical and numerical approaches

Hakim Amara,[1,2,*] Jaysen Nelayah,[2] Jérôme Creuze,[3] Adrian Chmielewski,[2] Damien Alloyeau,[2] Christian Ricolleau,[2] and Bernard Legrand[4]

[1]*Laboratoire d'Etude des Microstructures, ONERA-CNRS, UMR104, Université Paris-Saclay, BP 72, Châtillon Cedex, 92322, France*
[2]*Université de Paris, Laboratoire Matériaux et Phénomènes Quantiques (MPQ), F-75013, Paris, France*
[3]*ICMMO, Université Paris Saclay, UMR 8182, Bât. 410, F-91405 Orsay Cedex, France*
[4]*Université Paris-Saclay, CEA, Service de Recherches de Métallurgie Physique, 91191 Gif-sur-Yvette, France*

(Received 30 July 2021; revised 3 December 2021; accepted 7 March 2022; published 4 April 2022)

Surface energy is a key quantity that controls many physical properties of materials, yet determining its value at the nanoscale remains challenging. By using *N*-body interatomic potentials and performing analytical calculations, we develop a robust approach to determine the surface energy of metallic nanoparticles as a function of particle size and temperature. A strong increase in the surface energy is obtained when the size of the nanoparticle decreases in both the solid and liquid states. However, we show how the use of the classical spherical approximation to characterize the surface area of a nanoparticle leads to an almost constant surface energy with size as usually done to characterize the thermodynamic and kinetic properties of NPs in many works. We then propose a correction of the spherical approximation that is particularly useful for small size nanoparticles to improve the different models developed in the literature so far.

DOI: 10.1103/PhysRevB.105.165403

I. INTRODUCTION

Surface energy (γ) is an important descriptor of metallic nanoparticles (NPs) as it drives, among others, their nucleation-growth mechanism, three-dimensional morphology, reactivity in various environments, surface segregation, and so on [1]. To characterize these wide range of phenomena, the main theories developed in the literature are derived from models that involve surface energies of infinite systems [2]. In other words, γ is basically assumed to be size independent. With this assumption, it is then possible to remarkably predict the equilibrium shape of free and supported crystallites based respectively on the Wulff and Wulff-Kaishew relations at the nanoscale [3–5]. Other examples illustrating the success of such a choice include understanding Ostwald's ripening during particle synthesis or annealing [6,7] and the reactivity of different metal facets to gas environments in catalytic processes [8]. From a fundamental point of view, this is very surprising because it is well known, both experimentally and theoretically, that many properties (thermodynamic, optical, and mechanical) of nanomaterials are strongly different from their bulk counterparts [9–14]. Despite the agreement of the different models employing the surface energy of the infinite system with the experimental observations, there is no direct evidence that the surface energy in case of NPs is indeed size independent. This is a very complicated issue to be addressed since there is not any clear and straightforward answer to it at present. Experimentally, no systematic studies on measurement of surface energy as a function of size are presented due to the extreme difficulty to measure absolute surface energy of very small NPs [15,16]. Theoretically, the existing literature contains many conflicting and contradictory results concerning the variation of the surface energy of metallic NPs with size. Actually, a simple dimensional argument is often put forward in the case of solid NPs [17,18]. According to this hypothesis, γ decreases with increasing size as the contribution of the different surface sites (vertices, edges), which are preponderant for small sizes, decreases at the expense of the facets. Although many studies agree with this trend [19–25], other suggest an opposite tendency [26–30]. Indeed, the dimensional argument is not that simple since γ is commonly defined as an excess energy with respect to a reference energy normalized to a surface area related to the NP. All the discrepancies are mainly due to the difficulty to correctly define the reference state to characterize the excess energy resulting from the presence of a surface and in particular the definition of the considered surface area [31,32]. In any scenario, it can be noted that there is no direct evidence that the surface energy remains constant with the size.

In this work, we investigate the surface energy of solid and liquid Cu NPs as a function of particle size with the aim to provide a robust γ calculation applicable to characterize the thermodynamic and kinetic properties of NPs through experimental or theoretical data. We focus on cuboctahedral NPs where an analytical study is possible, which is an asset of incomparable richness to the understanding of the numerical results. With our approach, the correlation between the effective area considered for γ calculation and its dependence on size is clearly demonstrated. Based on this statement, we demonstrate how a judicious and practical choice of NPs surface results in the independence of perfectly adapted to investigate the physical properties of NPs through different macroscopic models.

*hakim.amara@onera.fr

II. METHODOLOGY

We perform calculations at the atomic level for Cu NPs by using a specific N-body interatomic potential derived from the second moment approximation of the tight-binding scheme (TB-SMA) [33–35]. More details of the TB model can be found in Sec. I of the Supplemental Material [36]. Our TB framework gives direct access to the total energy of each atom. This possibility to easily analyze local energy distributions will be decisive in the following. The atomic interaction model is implemented in a Monte Carlo (MC) code in the canonical ensemble, based on the Metropolis algorithm, which allows us to relax the structures at finite temperatures [37]. In the canonical ensemble, MC trials correspond to random displacements. The average quantities are calculated over 10^6 MC macrosteps, a similar number of macrosteps being used to reach equilibrium. A MC macrostep corresponds to N propositions of random atomic displacement, N being the total number of atoms of the cluster. We consider cuboctahedral solid NP bounded by six squares and eight equilateral triangles which structure is constructed on the face-centered cubic (fcc) lattice, leading to the presence of outer facets of {100} and {111} orientations, respectively. From this structure, it is possible to define analytically all the sites for a given cluster size with k shells [18]. Indeed, this cluster contains 12 vertices (v), 24(k-1) atoms in edges (e), and 6(k-1)^2 and 4(k-2)(k-1) atoms on {100} and {111} facets (f), respectively. Moreover, the total number of atoms $N(k)$, the surface $S(k)$, and the volume $V(k)$ are given by the following equations::

$$N(k) = \frac{10}{3}k^3 + 5k^2 + \frac{11}{3}k + 1, \tag{1}$$

$$S(k) = 2(3+\sqrt{3})(kd)^2, \tag{2}$$

$$V(k) = \frac{5\sqrt{2}}{3}(kd)^3, \tag{3}$$

where d corresponds to the equilibrium distance between first neighbors. To characterize the evolution of surface energy of solid and liquid states, calculations are done at two temperatures (T= 5 and 1500 K). As seen in Sec. I of the Supplemental Material [36], the NPs are definitely in the liquid state for T= 1500 K. Intermediate temperatures were not considered because the presence of solid-liquid region at the transition makes the analysis very difficult. It is clear that the calculation of γ but also its definition is not so simple and is subject to considerable studies [38,39]. However, the main goal of the present work is essentially on providing a useful calculation for the exploitation of experimental or theoretical data to characterize the thermodynamic and kinetic properties of NPs. As a result, the so-called surface energy resulting from the creation of a surface is defined as an excess internal energy ($E_{\rm exc}$) normalized to a given surface area, A:

$$\gamma(R) = \frac{E_{\rm exc}}{A}, \tag{4}$$

where $E_{\rm exc} = E_{\rm NP}(R) - E_{\rm ref}$. $E_{\rm NP}(R)$ is the total energy of the NP of radius R where necessarily R and the number of k shells are linked. Last, $E_{\rm ref}$ is a reference energy to be defined. The calculation of $E_{\rm NP}(R)$ is not an issue since it is a straightforward output of the MC simulations. On the contrary, $E_{\rm ref}$ and A are not well-defined quantities. Typically the reference energy is commonly chosen as the energy of the bulk fcc in the solid state [23,31,40]. Regarding the surface area, its choice is not unique [32] and can strongly affect the results. To overcome this problem, we first consider the case of solid particles and then extend our approach to liquid systems.

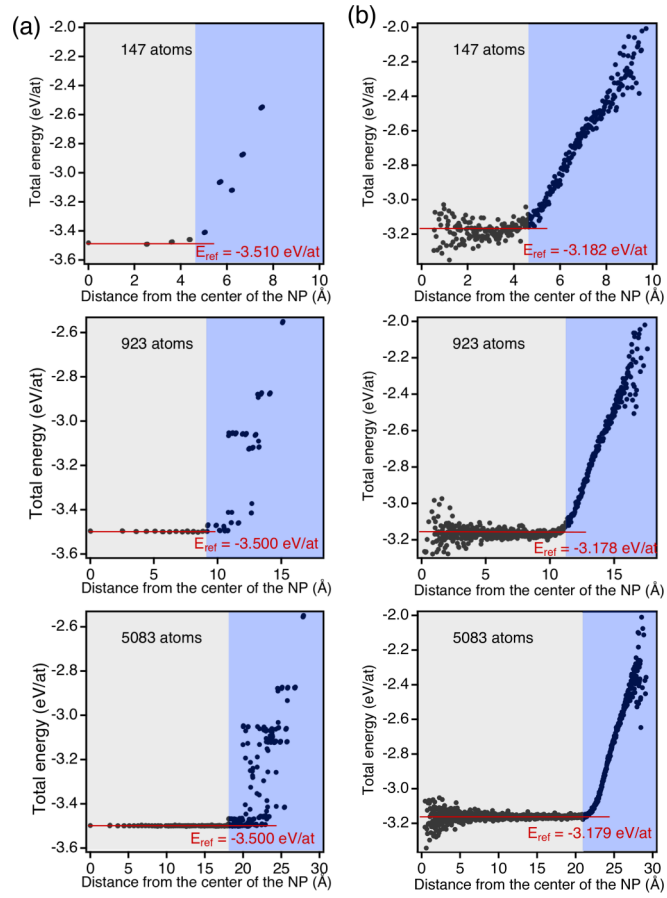

FIG. 1. Energy profiles along the radius of NPs containing 147, 923, and 5083 atoms (from top to bottom). Left: Solid NPs (T = 5 K); right: Liquid NPs (T = 1500 K). The gray and blue areas represent the core and surface atoms, respectively.

III. SOLID NANOPARTICLES

We apply two complementary approaches to get an insightful analysis of our results. The first is to calculate the surface energy from MC simulations according to Eq. (4) where $E_{\rm NP}$ (R) is obtained after relaxation at 5 K. The second one consists of developing an analytical model by assuming that all excess energy is ascribed to the surface sites [17,18]. This is made possible because all surface sites are perfectly identified. In both approaches, it is quite natural to consider A as the exact surface $S(k)$ of the cuboctahedral shape [see Eq. (2)]. Furthermore, the identification of local energies within the NP turns out to be very precious to tackle the challenge of correctly defining $E_{\rm ref}$. In Fig. 1(a), we present the energy profiles along the radius of the different nanoparticles (147, 923, and 5083 atoms) in solid state. Such an analysis is made possible by the calculation of local energies derived directly from the TB

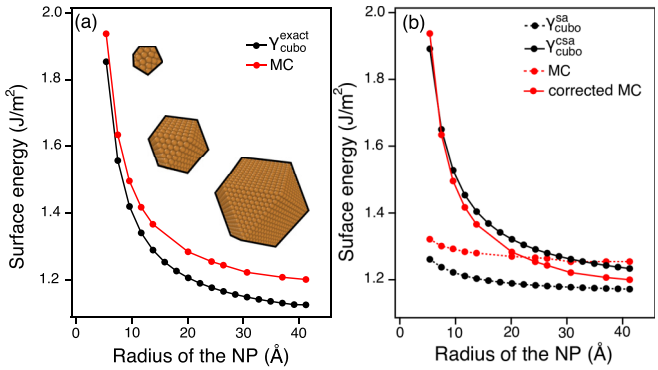

FIG. 2. Calculated surface energies for cuboctahedron Cu NPs as a function of size based on an (a) exact surface $S(k)$ and (b) a spherical (sa) approximation as well as corrected spherical approximation (csa). Both figures present analytical and MC results.

model. Interestingly, we can clearly identify two populations, i.e., core (gray area) and surface atoms (blue area). In case of solid NPs, the first corresponds to the core atoms which have energies around -3.50 eV/atom. The second population corresponds to surface atoms which are less stable and have energies reaching -2.60 eV/atom. The discontinuous aspect of the curve is mainly due to the layer structure of solid NP giving rise to this type of profile. Consequently, E_{ref} is simply the average energy of atoms identified in core position. In principle, it would be relevant to determine a different core energy for all sizes of NP. However, as the variation is very small (less than 10 meV/atom between Cu_{147} and Cu_{5083}), we choose to determine E_{ref} from the largest NP where the plateau corresponding to the core atoms is more clearly defined. In case of solid NP, E_{ref} is equal to -3.50 eV/at which is exactly the total energy per atom of a face-centered cubic bulk Cu in our TB model. This result confirms that defining E_{ref} from the bulk system, as done in many works, is completely justified.

At this stage, all the quantities required to determine $\gamma(R)$ from MC simulations according to Eq. (4) are known. The calculated surface energies for the cuboctahedral Cu NP as a function of size are shown in Fig. 2(a). It can be seen that the surface energy decreases with particle size. More precisely, there is a significant variation for small particles (<20 Å), from 1.92 to 1.22 J/m^2. For larger particles, the decrease of γ with the size becomes negligible to reach a constant value around 1.20 J/m^2. We now consider an analytical model where the determination of $\gamma(k)$ is simply reduced to the following equation:

$$\gamma_{\text{cubo}}(k) = \frac{\sum_i n_i \gamma_i}{A}, \tag{5}$$

where γ_i represents the local excess energy for each surface sites i $(i = v, e, f)$ defined as $E_i - E_{\text{ref}}$ and n_i being the number of sites of type i. In this approach, it is assumed that the excess energy is located only on the surface sites. The slice view shown in Fig. 3 provides a direct insight into the distribution within the nanoparticle and confirms the presence of two populations where the excess energy is located at the surface. Although subsurface atoms have still a slightly different energy than in bulk, we consider that they do not play a decisive role and that they can be neglected in γ

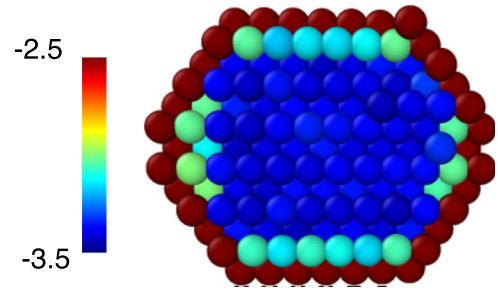

FIG. 3. Slice views showing the presence of core and surface populations for NPs containing 923 atoms in solid state where the contribution of subsurface atoms can be identified. Energies are in eV.

calculations. In a first step, A is considered as the exact surface $S(k)$ of the cuboctahedral NP [see Eq. (2)], and the related surface energy is noted $\gamma_{\text{cubo}}^{\text{exact}}(k)$. Meanwhile, the local energies of all sites (E_i) are calculated from our TB potential. As seen in Fig. 4, we plot the histogram of local energies for Cu NPs with total number of atoms, $N = 147$, 923, and 5083 atoms. Different populations of atoms can be identified [Fig. 4(a)]. The energies lie between -3.6 and -3.4 eV/atom are due to the bulk atoms which have 12 neighbors. The second population corresponds to the surface atoms which energies are below -3.2 eV/atom. As expected, the contribution of surface atoms decreases as the cluster size increases from Cu_{147} to Cu_{5083}. Moreover, a local analysis presented in Fig. 4(b) provides a spatial representation of the different surface sites with the following hierarchy: $E_{\{111\}} < E_{\{100\}} < E_e < E_v$. This result is not surprising since it is directly related to the coordination number (Z_i) of each site. The larger Z_i is, the higher the cohesion energy. Finally, it is particularly interesting to note that local energies are independent on the size and remain constant whatever the nanoparticle under consideration. From this local analysis, the resulting values of γ_i are presented in Table I. From $\gamma_{\text{cubo}}^{\text{exact}}(k)$, the analytically calculated surface energy for the cuboctahedral Cu NPs as a function of size

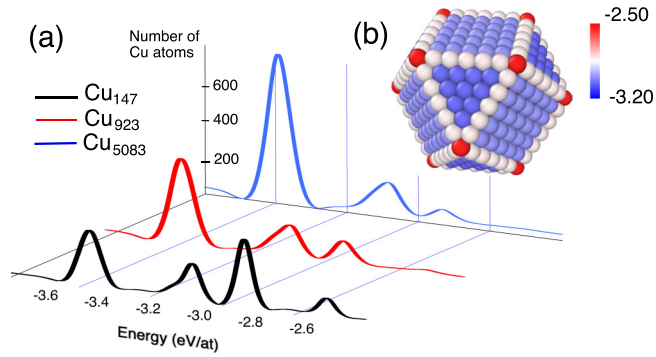

FIG. 4. (a) Analysis of the local energies in a histogram form for Cu solid NPs containing 147, 923, and 5083 atoms at 5K. For the sake of clarity, the values for the number of atoms in case of the NP_{147} have been increased by a factor of 10. (b) Analysis of the local energies on surface sites of solid Cu_{923} NP where different populations can be identified according to the following hierarchy: $E_f < E_e < E_v$. Note that the distinction between the different facets ({111} and {100}) is not visible at this scale. Energies are in eV/at.

TABLE I. Local excess energy for each surface site and crucial quantities that are involved in the calculation of $\gamma_{\text{cubo}}^{\text{exact}}(k)$ and $\gamma_{\text{cubo}}^{\text{sa}}(k)$. Values are given in eV for all noble metals.

	γ_v	γ_e	γ_{100}	γ_{111}	$2\gamma_e - \gamma_{100} - \gamma_{111}$	$2\gamma_e - \frac{3}{2}\gamma_{100} - \frac{4}{3}\gamma_{111}$
Cu	0.94	0.62	0.43	0.37	0.44	0.09
Ag	0.60	0.38	0.28	0.22	0.26	0.05
Au	0.56	0.36	0.29	0.21	0.22	0.005

is shown in Fig. 2(a). Similarly to results obtained from MC simulations, the surface energy decreases strongly with size. Moreover, results from the analytical model are in good agreement with the complete MC calculations, the small difference observed being due to the the subsurface contributions. To go deeper and analyze this tendency, the first-order Taylor expansion of $\gamma_{\text{cubo}}^{\text{exact}}(k)$ turns out to be very precious (see details in Sec. II of the Supplemental Material [36]):

$$\gamma_{\text{cubo}}^{\text{exact}}(k) \approx \gamma_{\infty}^{\text{exact}} + \frac{6[2\gamma_e - \gamma_{100} - \gamma_{111}]}{kd^2(3+\sqrt{3})}$$

$$\gamma_{\infty}^{\text{exact}} = \frac{3\gamma_{100} + 2\gamma_{111}}{d^2(3+\sqrt{3})}, \tag{6}$$

where $\gamma_{\infty}^{\text{exact}}$ corresponds to the plateau observed in Fig. 2 for large NPs [i.e., for $k \to \infty$ in Eq. (6)]. In addition, the second term is necessarily positive according to the γ_i hierarchy discussed above. As seen in Table I, this argument is valid for all noble metals. Consequently, the heterogeneity of the surface with different types of site explains the decrease in $\gamma(R)$, as already argued in previous works with a simple dimensional argument [17,18].

On a purely theoretical point of view, it is quite natural to consider the true surface of the cuboctahedron $S(k)$ as done so far. Experimentally, it is, however, not always possible to identify the exact shape of the NP (i.e., icosahedron, decahedron, and cuboctaedron) and even less to determine the exact surface area of the observed NPs. In practice, a spherical approximation of the different NPs to be analyzed is made. Typical examples from transmission electron microscopy (TEM) images are presented in Fig. 5(a) where a radius R can be assigned to each NPs in solid states (see Sec. III of the Supplemental Material for experimental details [36]). Within this spherical approximation, determining A of a solid NP from MC simulations is also nontrivial. Actually, the effective surface is equal to $4\pi R^2$. To address the arising difficulty in MC simulations, R is determined from the atomic density, $\rho_{\infty} = \sqrt{2}/d^3$ (see Sec. IV of the Supplemental Material [36]) using the following relation: $R^3(k) = 3N(k)/4\pi\rho_{\infty}$. To highlight the relevance of such a choice, Fig. 5(a) shows the sphere obtained from ρ_{∞} on snapshots of MC simulations from solid NPs, whose surface area is noted $S^{\text{sa}}(k)$. The comparison with the determination of the radius of the NPs from TEM images is clearly relevant. From Eq. (4), it is now possible to calculate the dependency with the size of the surface energy within the spherical approximation from MC simulations. As seen in Fig. 2(b), the conclusion differs significantly from the exact calculation. Indeed, almost no variation is observed and γ remains rather constant around

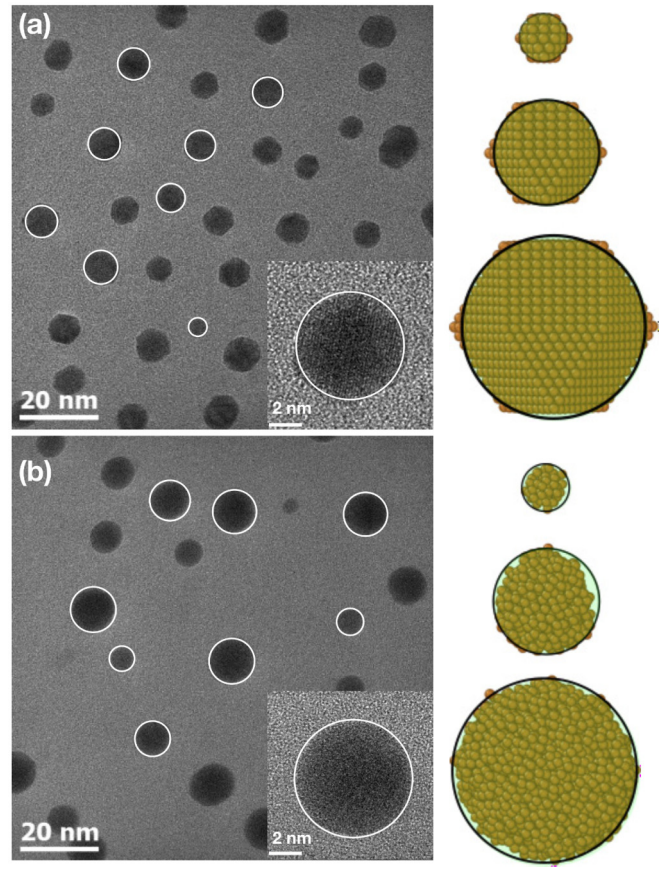

FIG. 5. Spherical approximation to determine the effective surface area from TEM images of Cu NPs in (a) solid (facetted NPs at 573 K) and (b) liquid states (nonfaceted NPs with a spherical shape at 1073 K). On the right: Comparison of the sphere of radius R obtained from the atomic density (ρ_{∞}) with configurations from MC simulations for different sizes and states of NPs containing 55 atoms, 561 atoms, and 2869 atoms. For the liquid cases, it is obvious that a snapshot is not so representative of the situation since the particle is strongly deformed during the simulation.

1.23 J/m^2. Consequently, the surface energy using the spherical approximation does not depend on the size of the system. In fact, the apparent discrepancy between the two approaches can be attributed to the different ways to calculate the surface area. Once the gap between both approaches becomes negligible, then an equivalent behavior can be observed where the surface energy varies only slightly (see Fig. 6). Obviously, this happens for sufficiently large particles where the spherical approximation is all the more adapted. To better understand these differences with the strong decrease observed for $\gamma_{\text{cubo}}^{\text{exact}}(k)$, a first-order Taylor expansion of $\gamma(k)$ within the spherical approximation (sa), noted $\gamma_{\text{cubo}}^{\text{sa}}(k)$, is done leading to (see Sec. V of the Supplemental Material [36]):

$$\gamma_{\text{cubo}}^{\text{sa}}(k) \approx \gamma_{\infty}^{\text{sa}} + \frac{6[2\gamma_e - (3/2)\gamma_{100} - (4/3)\gamma_{111}]}{kd^2(25\pi)^{1/3}}$$

$$\gamma_{\infty}^{\text{sa}} = \frac{3\gamma_{100} + 2\gamma_{111}}{d^2(25\pi)^{1/3}}. \tag{7}$$

As seen in Fig. 2(b), we confirm an almost constant variation of $\gamma(k)$ around 1.20 J/m^2. Such observation is in agreement

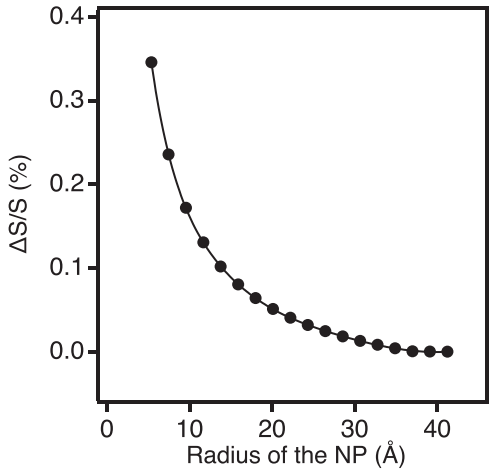

FIG. 6. Relative difference between the surface area calculated according to the spherical approximation and the exact one of the cuboctahedron as a function of size.

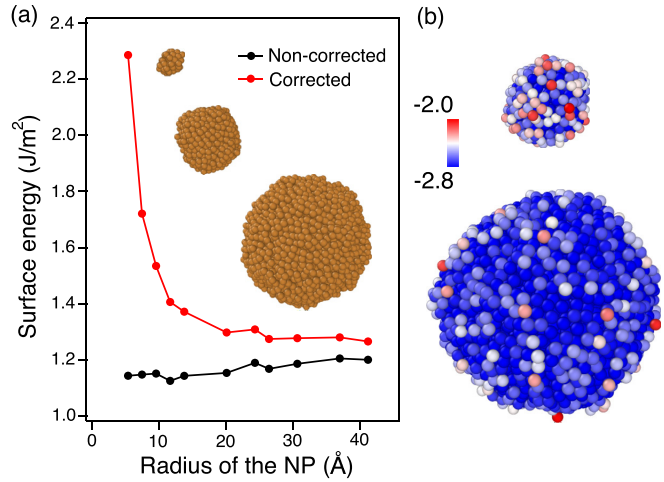

FIG. 7. (a) Calculated surface energies for liquid Cu NPs as a function of size within a spherical approximation and corrected spherical approximation. (b) Analysis of the local energies on surface of liquid NPs containing 561 and 5083 atoms. Energies are in eV.

with MC simulations where the discrepancy in the plateau is mainly due to the assumption of considering only surface sites in the analytical approach. Unfortunately, the variation of γ with size is not straightforward contrary to the exact calculation discussed previously. Indeed, nothing can be concluded about the importance of the predominant term in the numerator of Eq. (7). In the particular case of Cu, it is close to zero explaining the stability of γ with size. To generalize this result, the estimation of the numerator has been extended to other noble metals (Ag and Au) confirming this trend (see Table I). Within the spherical approximation, our analytical calculations therefore suggest that the surface energy does not vary with the size and is equal to $\gamma_{\infty}^{\mathrm{sa}}$ [i.e., for $k \to \infty$ in Eq. (7)].

In the following, we analyze the error made in the spherical approximation where two strong assumptions were established. The first one was to determine $R(k)$ from the atomic density where all the atoms constituting the NP contribute equally. However, as seen in Sec. IV of the Supplemental Material [36], ρ_{∞} is correctly reproduced (at least to first order) when only considering that the surface atoms, $N_{\mathrm{surf}}(k)$, contribute half compared to the core atoms. In the definition of $R(k)$, this is equivalent to consider that the total number of atoms is $N(k) - N_{\mathrm{surf}}(k)/2$. In this corrected spherical approximation (csa), the surface area becomes $S^{\mathrm{csa}}(k) = S^{\mathrm{sa}}(1 - 1/k)$. By applying this new surface formulation to the MC simulations, a significant variation of the surface energy with the size of the NPs is found. The result (corrected MC) presented in the Fig. 2(b) shows a decrease for NPs smaller than 20 Å to reach a plateau in the order of 1.20 J/m^2. As seen in Fig. 2(b), the same trend is observed for the analytical model, $\gamma_{\mathrm{cubo}}^{\mathrm{csa}}(k)$, where $S^{\mathrm{csa}}(k)$ is considered. In other words, by using this simple surface area correction to the spherical approximation, it is possible to restore the energy dependence obtained with an exact description of the surface area. The second assumption comes from the morphology, i.e., sphere rather than cuboctahedron. Actually, the following relationship $\gamma_{\mathrm{cubo}}^{\mathrm{csa}}(k) \approx 1.10\gamma_{\mathrm{cubo}}^{\mathrm{exact}}(k)$ can be established (see Sec. V of the Supplemental Material [36]). Thereby, the only difference between the exact calculation and the corrected spherical approximation ones results in a morphological factor due to the difference between a sphere and a cuboctahedron. To conclude, the spherical approximation is very appropriate for large sizes (with a constant form factor) but must be corrected for small sizes by a factor modifying the radius of the NP, which itself depends on the size and takes into account the specific contribution of the surface atoms.

IV. LIQUID NANOPARTICLES

Let us now consider liquid NPs by applying the approach developed for solid NPs to determine E_{ref} and A in Eq. (4). For the reference energy, it is simply a question of calculating the average energy of a bulk system at 1500 K. From the energy profiles presented in Fig. 1(b), E_{ref} is equal to -3.18 eV/at and corresponds to an infinite system in the liquid state at 1500 K. To determine the surface area, one can no longer rely on an exact calculation. Moreover, the corrected spherical approximation allows a precise determination of this area by assuming that the number of surface atoms is very close to that in the solid state. Meanwhile, the usual spherical approximation is subject to the same disadvantage as in the solid state, i.e., an overestimation of the volume (and therefore of the radius) of the NP at small sizes, which is even greater the smaller the size is. Figure 7(a) shows that the variation of the surface energy with the size of the NP in the liquid state is very similar to that observed in the solid state. Thus the calculation with the usual spherical approximation shows a constant surface energy close to 1.15 J/m^2, whereas the corrected spherical approximation gives a strong increase of γ when the size decreases, a variation slightly higher than that observed in the solid state. This significant variation may seem very surprising if we refer to the solid state where the weight of highly energetic sites (edges and vertices) decreases in favor of that of the facets when the size increases. However, vertices, edges, and facets no longer exist in the liquid state

and it is tempting to think that the surface energy distribution is relatively homogeneous. To address this issue, we determined the local energies in terms of spatial distribution in the liquid state. As seen in Fig. 7(b), we show the local energies for two NP sizes (561 and 5083 atoms). The particles do adopt a quasispherical shape without the presence of facets and edges in agreement with TEM observations [see Fig. 5(a)]. Nevertheless, the energy analysis shows a strong surface heterogeneity. There is a difference of about 0.8 eV between the most energetic and the least energetic surface atoms, compared to a difference of about 0.6 eV in the solid state between vertices and facets {111}. This unexpected presence in the liquid state of highly energetic surface atoms whose weight decreases with increasing size [cf. Fig. 7(b)] is at the origin of the strong variation of γ with size, as in the solid state. Note that all snapshots analyzed for the different sizes considered in this study exhibited this strong disparity with the presence of high-energy sites. The determination of the statistics of these sites as a function of size and temperature remains to be done through an analysis of the average energy distributions (see Sec. VI of the Supplemental Material [36]). While relevant, this is beyond the scope of the present study. As proposed in case of solid NPs, this result therefore suggests that a heterogeneous surface necessarily tends to a variation in the value of γ.

V. CONCLUSION

Based on both numerical simulations and analytical developments, this study explains the origin of the disagreements regarding the evolution of the surface energy with the size of the NPs [19–21,25,28,32]. Our microscopic approach being direct, it allows us to go beyond the approximations or parameters that are present in many works in the literature ranging from an atomistic description [21,25,40] to macroscopic models. For the latter, the work of Tolman [41,42], which is an extension of a development based on Gibbs theory [43], stands as a reference. From a macroscopic thermodynamic point of view, this formalism gives an expression of the variation of the surface tension γ of a spherical liquid droplet as a function of its radius by introducing a characteristic length, δ, called the Tolman length [44,45]. It is defined as the difference between the radii of the equimolar dividing surface (R_e) and the surface of tension (R_s) of the droplet. The position of the equimolar surface is defined when the chemical potential of the liquid and the gas phases are equal. Unfortunately, this macroscopic model is not adapted to describe the surface energy at the nanoscale since it involves phenomenological quantities (R_e, R_s) that are difficult to justify (or define) even at the microscopic level. As a result, our unique approach thus unifies numerous works and approaches in the literature. A strong dependence is obtained when the exact surface of the NP is considered, which is possible for simple forms. In contrast, using the classical spherical approximation, we obtain a surface energy that is almost independent of the size of the NP. If we correct the classical spherical approximation by taking into account the specific contribution of the surface atoms, we obtain a very good agreement with the exact calculation within one morphological factor. This result is particularly useful for dealing with liquid NPs, for which the exact surface area can hardly be calculated. Moreover, density functional theory calculations can be used to determine γ, either by considering the exact area when possible or by using the corrected spherical approximation. The findings reported here for cuboctrahedron NPs may be transferable to experimentally observed shapes (truncated octahedra, decahedra, and so on) which are also bounded by {111} and/or {001} facets. In the particular case of icosahedral NPs, the excess energy is localized at the surface as well as in the core of the NP making the generalization of our approach more delicate or even impossible. How then can we explain the success of thermodynamic or kinetic approaches that use the classical spherical approximation and that reproduce well the experimental data, while neglecting the variation of γ with size [3–8] The answer is that they rely on the expression of the chemical potential which involves the product γA and where the excess energy of the NP is considered to be localized at the surface (and does not contain core contributions as for the icosahedron). In these approaches, it is therefore essential to respect the consistency of the calculations of γ and A. This product can be evaluated either by considering the exact value of the surface area A and the exact variation of γ with size, or by considering the value of A given by the classical spherical approximation and the value of γ consistent with this calculation of A, namely a constant value equal to that of a semi-infinite bulk. In this latter case, even if the variations of γ and A are not exact, the product is correct explaining the success of thermodynamic or kinetic approaches based on the classical spherical approximation.

To conclude, we present a robust and direct method to calculate the surface energy of metallic nanoparticles of different sizes in the solid (here with cuboctahedron shape) and liquid states to reconcile the apparently contradictory results described in the literature. By considering an exact surface of the NP, we show that a significant dependence on size is obtained with a strong increase of the surface energy when the size of the NP decreases. In contrast, using the classical spherical approximation to characterize the surface area, we obtain a surface energy almost independent of the size of the NP for solid and liquid states. Such a discrepancy does not come from the morphology (sphere vs. cuboctahedron) but from the definition of the radius of the considered NPs. To overcome this problem, we propose for the first time a simple way to introduce a corrective term allowing to restore a strong variation of the surface energy from the spherical approximation. In contrast to previous works in the literature, we sought to develop an approach that could be applied to experimental data and used in thermodynamic and/or kinetic models. Indeed, the use of the spherical approximation being simpler in practice for the analysis of experimental data (as shown in our work from transmission electron microscopy images) or for theoretical developments, it then becomes possible to improve the models used so far to better characterise the thermodynamic and kinetic properties of NPs. Moreover, the interpretations and the correction presented in this manuscript can be applied to the surface energy of any metallic NP whatever the state and for different shapes. Our work thus is an advance in understanding likely to influence thinking in the field and represents a significant step towards understanding the unique properties of nano-objects.

ACKNOWLEDGMENTS

The support from the French research funding agency (ANR) under Grant No. 18-CE09-0014-01 (GIANT) is gratefully acknowledged. The authors are grateful to Région Ile de France for convention SESAME E1845 for the support of the JEOL electron microscope installed at Université de Paris. J.N. acknowledges funding from the French National Research Agency through the TOTEM project, Grant No. ANR-17-CE07-0031. H.A. and B.L. thank F. Ducastelle for fruitful discussions.

[1] L.-B. He, L. Zhang, L.-P. Tang, J. Sun, Q.-B. Zhang, and L.-T. Sun, Novel behaviors/properties of nanometals induced by surface effects, Mater. Today Nano **1**, 8 (2018).

[2] L. Vitos, A. V. Ruban, H. L. Skriver, and J. Kollár, The surface energy of metals, Surf. Sci. **411**, 186 (1998).

[3] G. Wulff, Zur frage der geschwindigkeit des wachsthums und der auflösung der krystallflächen, Z. Kristallogr. **34**, 449 (1901).

[4] R. Kaishew, Comm. Bulg. Acad. Sci. **1**, 100 (1950).

[5] C. R. Henry, Morphology of supported nanoparticles, Prog. Surf. Sci. **80**, 92 (2005).

[6] D. Alloyeau, G. Prévot, Y. Le Bouar, T. Oikawa, C. Langlois, A. Loiseau, and C. Ricolleau, Ostwald Ripening in Nanoalloys: When Thermodynamics Drives a Size-Dependent Particle Composition, Phys. Rev. Lett. **105**, 255901 (2010).

[7] G. Prévot, N. T. Nguyen, D. Alloyeau, C. Ricolleau, and J. Nelayah, Ostwald-driven phase separation in bimetallic nanoparticle assemblies, ACS Nano **10**, 4127 (2016).

[8] A. Chmielewski, J. Meng, B. Zhu, Y. Gao, H. Guesmi, H. Prunier, D. Alloyeau, G. Wang, C. Louis, L. Delannoy, P. Afanasiev, C. Ricolleau, and J. Nelayah, Reshaping dynamics of gold nanoparticles under H_2 and O_2 at atmospheric pressure, ACS Nano **13**, 2024 (2019).

[9] Ph. Buffat and J-P. Borel, Size effect on the melting temperature of gold particles, Phys. Rev. A **13**, 2287 (1976).

[10] D. Alloyeau, C. Ricolleau, C. Mottet, T. Oikawa, C. Langlois, Y. Le Bouar, N. Braidy, and A. Loiseau, Size and shape effects on the order-disorder phase transition in CoPt nanoparticles. Nat. Mater. **8**, 940 (2009).

[11] L. Delfour, J. Creuze, and B. Legrand, Exotic Behavior of the Outer Shell of Bimetallic Nanoalloys, Phys. Rev. Lett. **103**, 205701 (2009).

[12] Y. Magnin, A. Zappelli, H. Amara, F. Ducastelle, and C. Bichara, Size Dependent Phase Diagrams of Nickel-Carbon Nanoparticles, Phys. Rev. Lett. **115**, 205502 (2015).

[13] F. T. Rabouw and C. De Mello Donega, Excited-state dynamics in colloidal semiconductornanocrystals. Top. Curr. Chem. (Z) **374**, 58 (2016).

[14] D. Guo, G. Xie, and J. Luo, Mechanical properties of nanoparticles: Basics and applications, J. Phys. D: Appl. Phys. **47**, 013001 (2013).

[15] K. K. Nanda, A. Maisels, F. E. Kruis, H. Fissan, and S. Stappert, Higher Surface Energy of Free Nanoparticles, Phys. Rev. Lett. **91**, 106102 (2003).

[16] A. Chmielewski, J. Nelayah, H. Amara, J. Creuze, D. Alloyeau, G. Wang, and C. Ricolleau, Direct Measurement of the Surface Energy of Bimetallic Nanoparticles: Evidence of Vegard's Rulelike Dependence, Phys. Rev. Lett. **120**, 025901 (2018).

[17] A. Perini, G. Jacucci, and G. Martin, Interfacial contribution to cluster free energy, Surf. Sci. **144**, 53 (1984).

[18] T. P. Martin, T. Bergmann, H. Goehlich, and T. Lange, Shell structure of clusters, J. Phys. Chem. **95**, 6421 (1991).

[19] E. Müller, W. Vogelsberger, and H.-G Fritsche, The dependence of the surface energy of regular clusters and small crystallites on the particle size, Cryst. Res. Technol. **23**, 1153 (1988).

[20] B. Medasani, Y. H. Park, and I. Vasiliev, Theoretical study of the surface energy, stress, and lattice contraction of silver nanoparticles, Phys. Rev. B **75**, 235436 (2007).

[21] S. Xiong, W. Qi, Y. Cheng, B. Huang, M. Wang, and Y. Li, Modeling size effects on the surface free energy of metallic nanoparticles and nanocavities, Phys. Chem. Chem. Phys. **13**, 10648 (2011).

[22] Cun Zhang, Yin Yao, and Shaohua Chen, Size-dependent surface energy density of typically fcc metallic nanomaterials, Comput. Mater. Sci. **82**, 372 (2014).

[23] S. Ali, V. S. Myasnichenko, and E. C. Neyts, Size-dependent strain and surface energies of gold nanoclusters, Phys. Chem. Chem. Phys. **18**, 792 (2016).

[24] V. S. Myasnichenko, M. Razavi, M. Outokesh, N. Yu Sdobnyakov, and M. D. Starostenkov, Molecular dynamic investigation of size-dependent surface energy of icosahedral copper nanoparticles at different temperature, Lett. Mater. **6**, 266 (2016).

[25] X. B. Jiang, B. B. Xiao, X. Y. Gu, and X. H. Zhang, Modeling the effects of size and surface broken bond on surface energy of nanocrystals, Thin Solid Films **640**, 67 (2017).

[26] H. M. Lu and Q. Jiang, Size-dependent surface energies of nanocrystals, J. Phys. Chem. B **108**, 5617 (2004).

[27] M. N. Magomedov, Dependence of the surface energy on the size and shape of a nanocrystal, Phys. Solid State **46**, 954 (2004).

[28] Y. Yao, Y. Wei, and S. Chen, Size effect of the surface energy density of nanoparticles, Surf. Sci. **636**, 19 (2015).

[29] Fahed M. Takrori and Ahmed Ayyad, Surface energy of metal alloy nanoparticles, Appl. Surf. Sci. **401**, 65 (2017).

[30] M. A. Jabbareh, Size, shape and temperature dependent surface energy of binary alloy nanoparticles, Appl. Surf. Sci. **426**, 1094 (2017).

[31] Y. Wei and S. Chen, Size-dependent surface energy density of spherical face-centered-cubic metallic nanoparticles, J. Nanosci. Nanotechnol. **15**, 9457 (2015).

[32] B. Molleman and T. Hiemstra, Size and shape dependency of the surface energy of metallic nanoparticles: Unifying the atomic and thermodynamic approaches, Phys. Chem. Chem. Phys. **20**, 20575 (2018).

[33] V. Rosato, M. Guillopé, and B. Legrand, Thermodynamical and structural properties of f.c.c. transition metals using a simple tight-binding model, Philos. Mag. A **59**, 321 (1989).

[34] J. Creuze, I. Braems, F. Berthier, C. Mottet, G. Tréglia, and B. Legrand, Model of surface segregation driving forces and their coupling, Phys. Rev. B **78**, 075413 (2008).

[35] F. Ducastelle, Module élastique des métaux de transition, J. Phys. (Paris) **31**, 1055 (1970).

[36] See Supplemental Material at http://link.aps.org/supplemental/10.1103/PhysRevB.105.165403 for details on the second moment approximation interatomic potential, Monte Carlo simulations, surface energy calculation using different approximations and experimental informations (TEM and synthesis), which includes Ref. [46].

[37] D. Frenkel and B. Smith, *Understanding Molecular Simulation* (Academic Press, London, 2002).

[38] S. W. Ip and J. M. Toguri, The equivalency of surface tension, surface energy and surface free energy, J. Mater. Sci. **29**, 688 (1994).

[39] P. Müller and A. Saúl, Elastic effects on surface physics, Surf. Sci. Rep. **54**, 157 (2004).

[40] D. Holec, P. Dumitraschkewitz, D. Vollath, and F. D. Fischer, Surface energy of Au nanoparticles depending on their size and shape, Nanomaterials **10**, 484 (2020).

[41] R. C. Tolman, Consideration of the Gibbs theory of surface tension, J. Chem. Phys. **16**, 758 (1948).

[42] R. C. Tolman, The effect of droplet size on surface tension, J. Chem. Phys. **17**, 333 (1949).

[43] J. W. Gibbs, *Collected Works* (Longmans Green and Company, New York, 1928).

[44] M. N. Joswiak, N. Duff, M. F. Doherty, and B. Peters, Size-dependent surface free energy and tolman-corrected droplet nucleation of tip4p/2005 water. J. Phys. Chem. Lett. **4**, 4267 (2013).

[45] X.-M. Ma, H.-T. Liang, W.-L. Lu, X. Zhang, Z.-Y. Yu, and Y. Yang, Atomistic characterization of the dispersed liquid droplet in immiscible al-pb alloy, J. Mater. Res. Technol. **15**, 2993 (2021).

[46] A. Chmielewski, C. Ricolleau, D. Alloyeau, G. Wang, and J. Nelayah, Nanoscale temperature measurement during temperature controlled in situ TEM using Al plasmon nanothermometry, Ultramicroscopy **209**, 112881 (2020).